Distinct sources of interannual subtropical and subpolar Atlantic overturning variability

Yavor Kostov[1], Helen L. Johnson[2], David P. Marshall[3]

Patrick Heimbach[4], Gael Forget[5], N. Penny Holliday[6], M. Susan Lozier[7],

Feili Li[7], Helen R. Pillar[4], Timothy Smith[4]

1. University of Exeter, Geography, Exeter, United Kingdom of Great Britain and Northern Ireland (y.kostov@exeter.ac.uk)
2. University of Oxford, Earth Sciences, Oxford, United Kingdom of Great Britain and Northern Ireland
3. University of Oxford, Physics, Oxford, United Kingdom of Great Britain and Northern Ireland
4. University of Texas at Austin, Oden Institute for Computational Engineering and Sciences, Austin, Texas, United States of America
5. Massachusetts Institute of Technology, Earth, Atmospheric, and Planetary Sciences, Cambridge, Massachusetts, United States of America
6. National Oceanography Centre, Southampton, United Kingdom of Great Britain and Northern Ireland
7. Georgia Institute of Technology, Earth and Atmospheric Sciences, Atlanta, Georgia United States of America

The Atlantic meridional overturning circulation (AMOC) is pivotal for regional and global climate due to its key role in the uptake and redistribution of heat and carbon. Establishing the causes of historical variability in AMOC strength on different timescales can tell us how the circulation may respond to natural and anthropogenic changes at the ocean surface. However, understanding observed AMOC variability is challenging because the circulation is influenced by multiple factors which co-vary and whose overlapping impacts persist for years. Here we reconstruct and unambiguously attribute intermonthly and interannual AMOC variability at two observational arrays

to the recent history of surface wind stress, temperature and salinity. We use a state-of-the-art technique that computes space- and time-varying sensitivity patterns of the AMOC strength with respect to multiple surface properties from a numerical ocean circulation model constrained by observations. While, on inter-annual timescales, AMOC variability at 26°N is overwhelmingly dominated by a linear response to local wind stress, overturning variability at subpolar latitudes is generated by the combined effects of wind stress and surface buoyancy anomalies. Our analysis provides a quantitative attribution of subpolar AMOC variability to temperature, salinity, and wind anomalies at the ocean surface.

Throughout the upper kilometer, the Atlantic meridional overturning circulation (AMOC) carries warm, high-salinity waters northward, while at depth it transports colder, low-salinity waters southward in a zonal mean sense (1). Coupled climate models suggest that the AMOC is likely to weaken over the coming decades, resulting in a decrease in the associated northward heat transport, with widespread implications for regional and global climate (2). Continuous observations of the AMOC since 2004 at 26°N, the location of the RAPID-MOCHA array, and since 2014 at subpolar latitudes, where the OSNAP array has been deployed, reveal large amplitude variability on all timescales accessible to date (3,4,5). Disentangling the roles of anomalies in wind stress and sea-surface temperature and salinity (SST and SSS) in driving historical AMOC variability has been a major obstacle, limiting our understanding of past changes and our ability to critically assess model predictions of the future of the overturning circulation. The fact that SST and SSS themselves respond to changes in the ocean circulation, which can be independent of local atmospheric forcing, makes distinguishing cause and effect even more challenging.

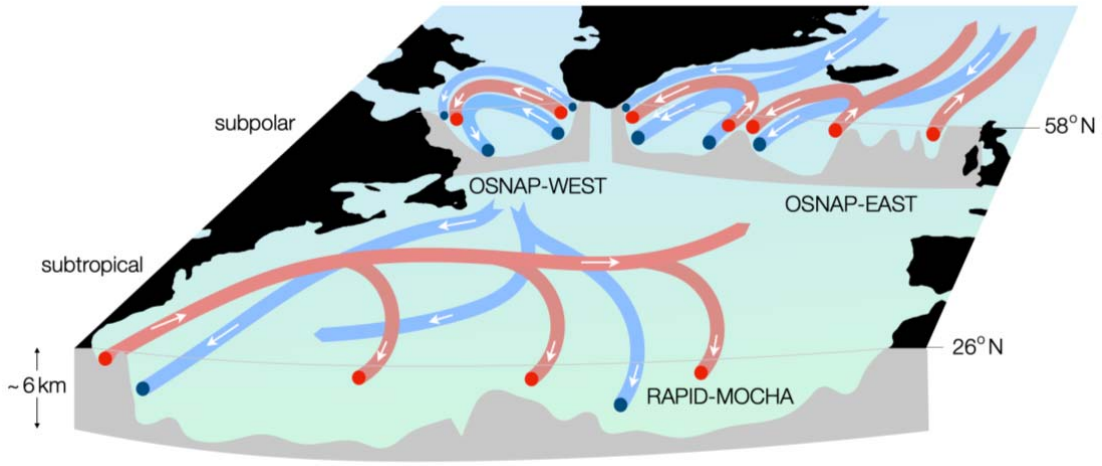

Figure 1. **Schematic of the large-scale ocean circulation in the subtropical and subpolar North Atlantic.** Colors differentiate major (red) warm, saline; and (blue) cool, fresh pathways of ocean currents. Bathymetric cross sections are shown in gray at the locations of the OSNAP-WEST, OSNAP-EAST, and RAPID-MOCHA arrays.

Attributing AMOC variability has traditionally been approached through perturbation experiments in climate models (6, 7). However, a prohibitively large number of perturbation simulations is necessary in order to fully resolve the spatially and seasonally-varying sensitivity of the AMOC to surface boundary conditions. Another standard method in attribution studies involves statistical analysis of the co-variability between the overturning circulation and surface properties such as air-sea heat flux, SST, SSS, and wind stress (7, 8). Still, many observables in the climate system co-vary and correlations among them do not reveal the direction of causality. Here we take a different approach towards attribution and use the adjoint (9,10) of an ocean model to establish unambiguous causal relationships (11, 12) between quantities at the air-sea interface and the lagged response of the AMOC. The adjoint of an ocean circulation model allows us to compute the sensitivity of a chosen metric, here the AMOC at a given latitude, to a range of variables, parameter choices, initial conditions and boundary conditions at various lead times (10, 11, 12). We use algorithmic

82 differentiation (13) to generate the adjoint (see Methods) of the ECCO version 4 (hereafter
83 ECCO) configuration (10, 14) of the MITgcm, a state-of-the art ocean general circulation model (15).
84 ECCO is an ocean state estimate, a data assimilation product in which a model simulation has been fit to
85 historical observations in a least-squares sense so as to best represent the evolution of ocean properties
86 over the period 1992-2015 (10, 14, 16, 17). ECCO skillfully reproduces measurements of temperature
87 and salinity (10, 14, 16, 17, 18), as well as the overturning circulation in the North Atlantic (See Figure
88 S1 in the SI).

89 Here we use this advanced computational framework to produce a quantitative attribution
90 of AMOC variability in the subpolar North Atlantic to anomalies in SST, SSS, and surface wind
91 stress at different lead times. We focus on OSNAP-EAST rather than OSNAP-WEST (Figure 1)
92 because the observed mean transport and variability in the Eastern Subpolar North Atlantic is greater and
93 is known to play an important role in the large-scale transformation from lighter into denser water masses
94 (19, 20, 21). We consider inter-monthly and inter-annual timescales and contrast the response of the
95 subpolar AMOC against that of the overturning across the RAPID-MOCHA mooring array at 26°N.

96 *Reconstruction of the OSNAP-EAST and RAPID-MOCHA AMOC*

97 We use the adjoint of the MITgcm ECCO configuration to isolate the sensitivity of the
98 overturning circulation to wind stress from its sensitivity to SST and SSS. This separation is
99 critical because changes in wind can lead to substantial anomalies in ocean temperature and
100 salinity. We then convolve these sensitivity patterns ($\mathcal{G}_{\mathcal{P}}$), which depend on the season, with
101 surface wind stress, SST, and SSS anomalies between 1992 and 2015 from the ECCO state
102 estimate. Each convolution provides an estimate for the time-evolving contribution C of the
103 anomaly in a particular ocean surface property $\mathcal{P}$ (temperature, salinity, or wind stress) to
104 historical variability in the rate of meridional overturning (the volume transport in Sverdrups,
105 where 1 Sv = 10^6 m^3s^{-1}):

$$C_{\mathcal{P}}(t) = \int_{t-\tau}^{t} \int \mathcal{P}(\boldsymbol{x}, t')\, \mathcal{G}_{\mathcal{P}}(t; \boldsymbol{x}, t - t')\, d\boldsymbol{x}\; dt', \qquad (1)$$

where $\mathcal{P}$ is the surface property anomaly relative to the climatology at a lead time t', up to a memory τ, and location $\boldsymbol{x}$; see Methods for further details. We sum the contributions from SST, SSS, and wind stress anomalies relative to the seasonal mean and then add the climatological seasonal cycle in overturning (11) from the ECCO state estimate. We thus reconstruct AMOC variability relative to the long-term mean at the latitudes of both the OSNAP-EAST and the RAPID-MOCHA arrays. We separately consider how individual sources of variability contribute to the total reconstruction. Furthermore, we explore how the seasonality in wind stress contributes to variability in the overturning relative to the long-term mean.

The reconstructed overturning variability across OSNAP-EAST (Figure 2a) is significantly correlated (R=0.69, and R=0.72 if we detrend the timeseries) with the historical overturning as represented in ECCO. The reconstruction of overturning variability at the latitude of the RAPID-MOCHA array (Figure 2b), based on surface wind stress, SST, and SSS, also shows good agreement with the ECCO state estimate (R=0.89) and with the direct observational estimate (R=0.70). Our reconstruction reproduces skillfully the sign, magnitude, and timing of the AMOC anomalies (Figure 2a,b). This high level of agreement suggests that AMOC variability is dominated by processes and mechanisms that our analysis largely captures.

The OSNAP-EAST observational record of 21 months is much shorter than that in the subtropical Atlantic, but first indications suggest that our reconstruction also captures some of the observed AMOC variability here. We interpolate our OSNAP-EAST reconstruction onto the same 30-day time windows as the direct observational estimate (See Extended Data Figure ED1). In 14 out of the 15 time windows where OSNAP-EAST observations and model output are both available, our envelope of reconstructions overlaps with the direct observational estimate within one standard error (See Extended Data Figure ED1). However,

over this short record, inter-monthly variability in our reconstructed OSNAP-EAST overturning is not positively nor significantly correlated with the observational time series.

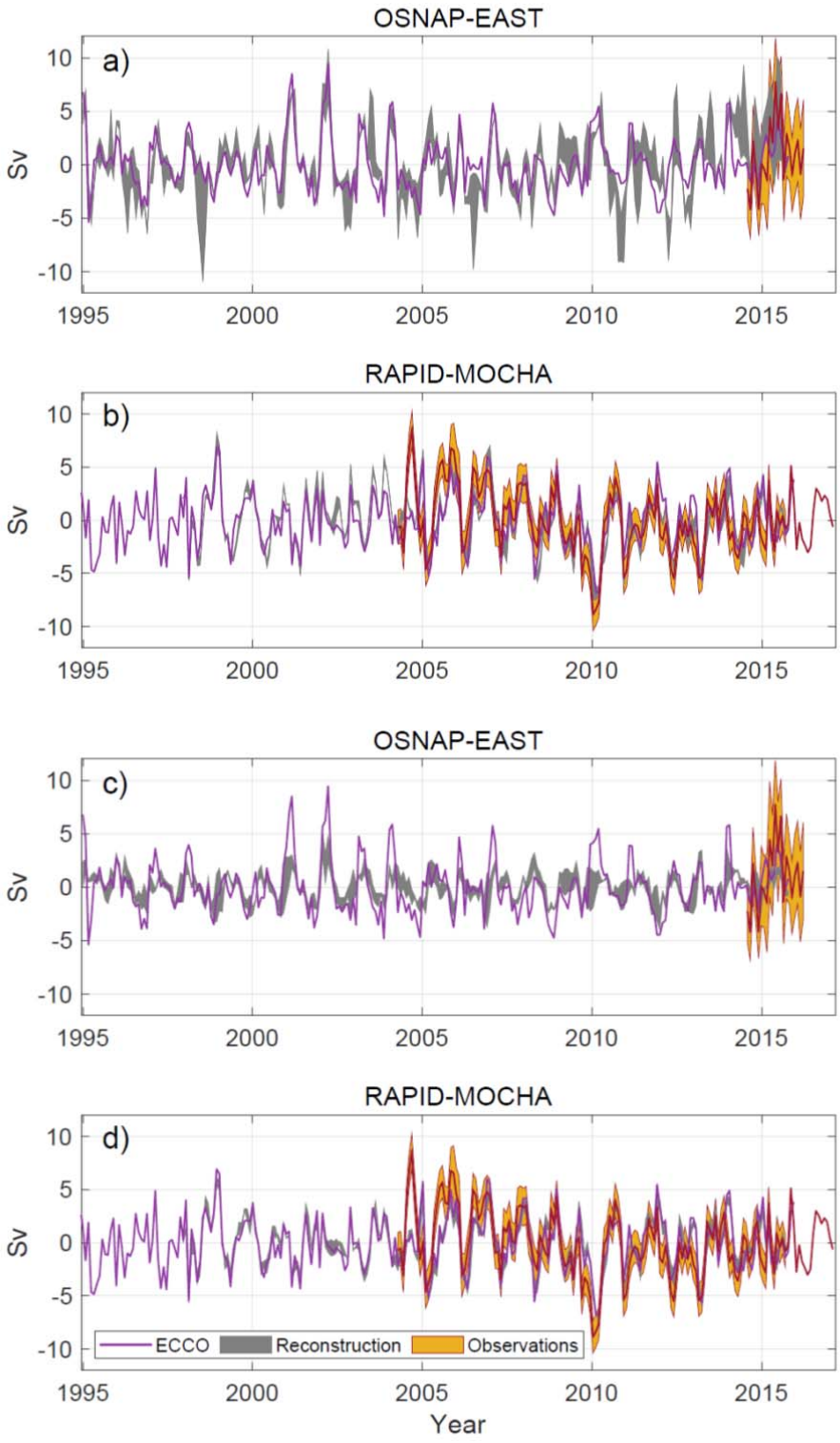
OSNAP-EAST
a)
RAPID-MOCHA
b)
OSNAP-EAST
c)
RAPID-MOCHA
d)
Sv
10
5
0
-5
-10
1995
2000
2005
2010
2015
Year
ECCO
Reconstruction
Observations

133

134

Figure 2. **Reconstruction of overturning in the North Atlantic.** Linear reeconstruction (gray) of variability in OSNAP-EAST (a,c) and RAPID-MOCHA (b,d) meridional overturning (volume transport in Sv) compared with the ECCO state estimate (purple) and the direct observational estimate (yellow and brown). Anomalies are shown relative to the long-term mean. The yellow shaded envelopes indicate ± 1 standard deviation of the observational uncertainty at OSNAP-EAST (see 19) and RAPID-MOCHA (See 35), and the thick brown lines show the mean estimates. The uncertainty of the observed RAPID-MOCHA overturning is not available for the last 17 months of the timeseries (the thick brown line in b and d). The reconstructions in a and b include contributions due to surface wind stress, SST, SSS, as well as the climatological seasonal cycle in overturning from ECCO. The thickness of the gray shading in a,b indicates the spread between two estimates of the reconstructed AMOC in ECCO, reflecting variability in the reference state about which the linearized reconstruction is computed (see Methods). The reconstructions in c,d show only contributions due to surface wind stress anomalies – including the contribution from the seasonal cycle – under fixed SST and SSS.

Nonlinearity in the sensitivity of the overturning circulation to surface forcing such as SST and SSS is a key potential source of uncertainty in our reconstructions. An important manifestation of nonlinearity in the overturning is the dependence of the sensitivity patterns, and hence the AMOC reconstructions, on the evolving background state of the ocean. For example, the exact sites of intense winter convection and deep water formation in the North Atlantic differ from one year to another. The gray shaded envelopes in Figure 2a,b show the spread in reconstructed AMOC variability that results from using sensitivity patterns computed over two different historical periods in ECCO: one ending in 2001-2002 and one in

159 2006-2007. (see Methods). This largely reflects changes in the sensitivity to wintertime
160 surface buoyancy anomalies between the two periods analyzed. This can be seen by
161 comparing the large spread in the full reconstruction that includes the buoyancy component (Fig
162 2a,b) to the diminished spread in the wind-only reconstruction (Fig 2c,d). The dependence on the
163 background state is more pronounced in the OSNAP-EAST timeseries than the subtropical
164 RAPID-MOCHA AMOC and explains the lower skill in recovering the subpolar overturning. In
165 addition, for numerical reasons, the adjoint of the model approximates the parameterization of
166 vertical mixing and sea ice physics, nonlinear processes that are very active in the high latitude
167 oceans and thus affect more strongly the OSNAP-EAST reconstruction compared to the RAPID-
168 MOCHA AMOC.
169
170 *Attribution of AMOC variability to wind, SST, and SSS*
171 Much of the variability (R=0.94) in historical overturning at 26°N can be explained in terms of wind-
172 driven circulation anomalies (Figure 2d and 4a,b; 11). A large fraction of the inter-monthly AMOC
173 anomalies at the RAPID-MOCHA array is attributed to processes within the surface Ekman
174 boundary layer (R=0.70, Extended Data Figure ED2), where there is a local balance between wind
175 stress and a component of the Coriolis force (22). Surface buoyancy anomalies contribute to low-
176 frequency variability in the subtropical AMOC, such as the reconstructed 2007-2011 decline in the
177 overturning at the RAPID-MOCHA array (Figure 3b). This historical weakening of the AMOC is
178 very pronounced in the observational time-series (4; Figure 2b) but less so in ECCO (Figure 2b),
179 possibly because high latitude density variability in the state estimate is biased relative to
180 observations (23).
181 Wind-induced variability, including the seasonal cycle in surface wind stress, also contributes
182 noticeably to anomalies in the overturning across OSNAP-EAST (R=0.68, Figure 2c). However, winds do

not overwhelmingly dominate the subpolar AMOC as they do at 26°N. If we consider only wind stress anomalies relative to the seasonal cycle, they explain 31% of the variability at OSNAP-EAST (R=0.56). Anomalies in SST and SSS relative to the seasonal cycle jointly explain a smaller but comparable fraction, 12% of variability (R=0.35) in the OSNAP-EAST AMOC as represented in ECCO. SST and SSS anomalies drive inter-annual variability in the OSNAP-EAST circulation that is similar in magnitude to the large background seasonal cycle in overturning (Figure 3a). All of these components – due to wind stress, SST, and SSS – combine to generate variability at the OSNAP-EAST array that can be largely explained by a geostrophic balance between the Coriolis force and pressure gradients even on inter-monthly timescales (Extended Data Figure ED3). We note that this is in contrast to variability at the RAPID-MOCHA line, where geostrophic balance dominates only at low frequencies (Extended Data Figure ED3, 4, 24, 25).

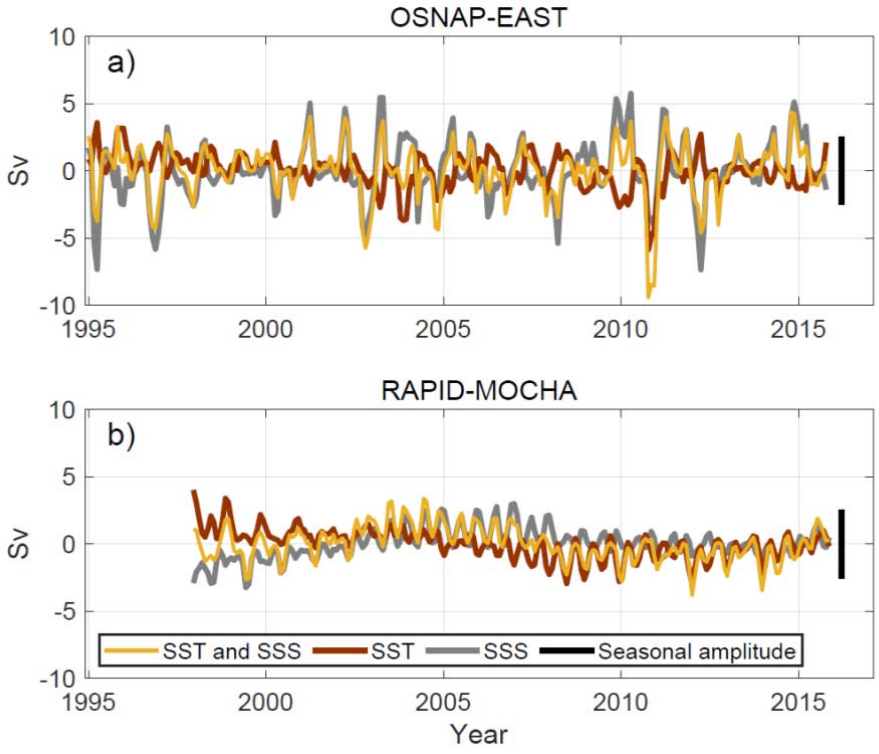

Figure 3. **Contributions of sea-surface salinity and temperature to variability in overturning**. Sea surface salinity (gray) and temperature (brown) contributions to

196 the total buoyancy component (yellow) of the OSNAP-EAST (a) and RAPID-AMOC
197 (b) reconstructions. The estimates use sets of sensitivity patterns based on a
198 linearization of the model over a single historical period (See Methods), while the full
199 reconstructions in Figure 2 use linearization over two historical periods to estimate
200 uncertainty. For comparison, vertical black bars indicate the amplitude of the
201 seasonal cycle in RAPID and OSNAP-EAST overturning in ECCO. The timeseries of
202 contributions to RAPID-MOCHA overturning begin in 1998 because a 6-year
203 memory of SST and SSS is required (See Methods), and the observationally
204 constrained state estimate begins in 1992.

205 At both subtropical and subpolar latitudes, SSS-induced AMOC variability is significantly
206 anti-correlated with SST-induced AMOC variability (Figure 3). To explore this relationship, we
207 consider the AMOC sensitivity to surface boundary conditions in particular periods of the ECCO
208 state estimate (See Methods). The estimated SST and SSS contributions to OSNAP-EAST
209 variability shown in Figure 3a are anticorrelated with R=-0.42. This statistical relationship indicates a
210 partial compensation between the SSS- and SST-driven contributions to historical AMOC changes.
211 Generally, the variability due to SSS dominates over that due to SST at OSNAP-EAST (Figure 3a),
212 while at 26°N this is not the case (Figure 3b).

213

214 *Spatial origins of AMOC variability*

215 Figure 4 shows the spatial origins of the AMOC variability that results from anomalies in zonal
216 wind stress (a,e), meridional wind stress (b,f), SST (c,g) and SSS (d,h). Plotted is the root-mean-
217 square contribution per unit area [Sv m^{-2}] to the convolutions in equation (1) over the period 1992-
218 2015:

$$C_{\mathcal{P}}(\boldsymbol{x}) = \frac{1}{A(\boldsymbol{x})}\sqrt{\frac{1}{(T_f \cdot \tau)}\sum_{t=0}^{T_f}\sum_{t'=\max(t-\tau,0)}^{t}\left[\mathcal{P}(\boldsymbol{x},t')\,\mathcal{G}_{\mathcal{P}}(t;\boldsymbol{x},t-t')\right]^2} \qquad (2)$$

where $A(\boldsymbol{x})$ is the horizontal surface area of the model grid cell in location $\boldsymbol{x}$, $\mathcal{P}$ represents the surface field anomalies relative to the climatology at a lead time t' summed up to a finite maximum memory τ. The function $\mathcal{G}_{\mathcal{P}}$ is the corresponding sensitivity pattern that depends on the season, the lead time t', and the geographical location $\boldsymbol{x}$ as in equation (1). We sum the convolution of $\mathcal{P}$ and $\mathcal{G}_{\mathcal{P}}$ until the end of the available timeseries $t = T_f$ and compute the root-mean-square (See Methods). In effect, the convolution in equation (2) allows us to identify the regions where variability in wind stress, SST, and SSS most strongly projects onto the corresponding AMOC sensitivity patterns and activates them (Figure 4).

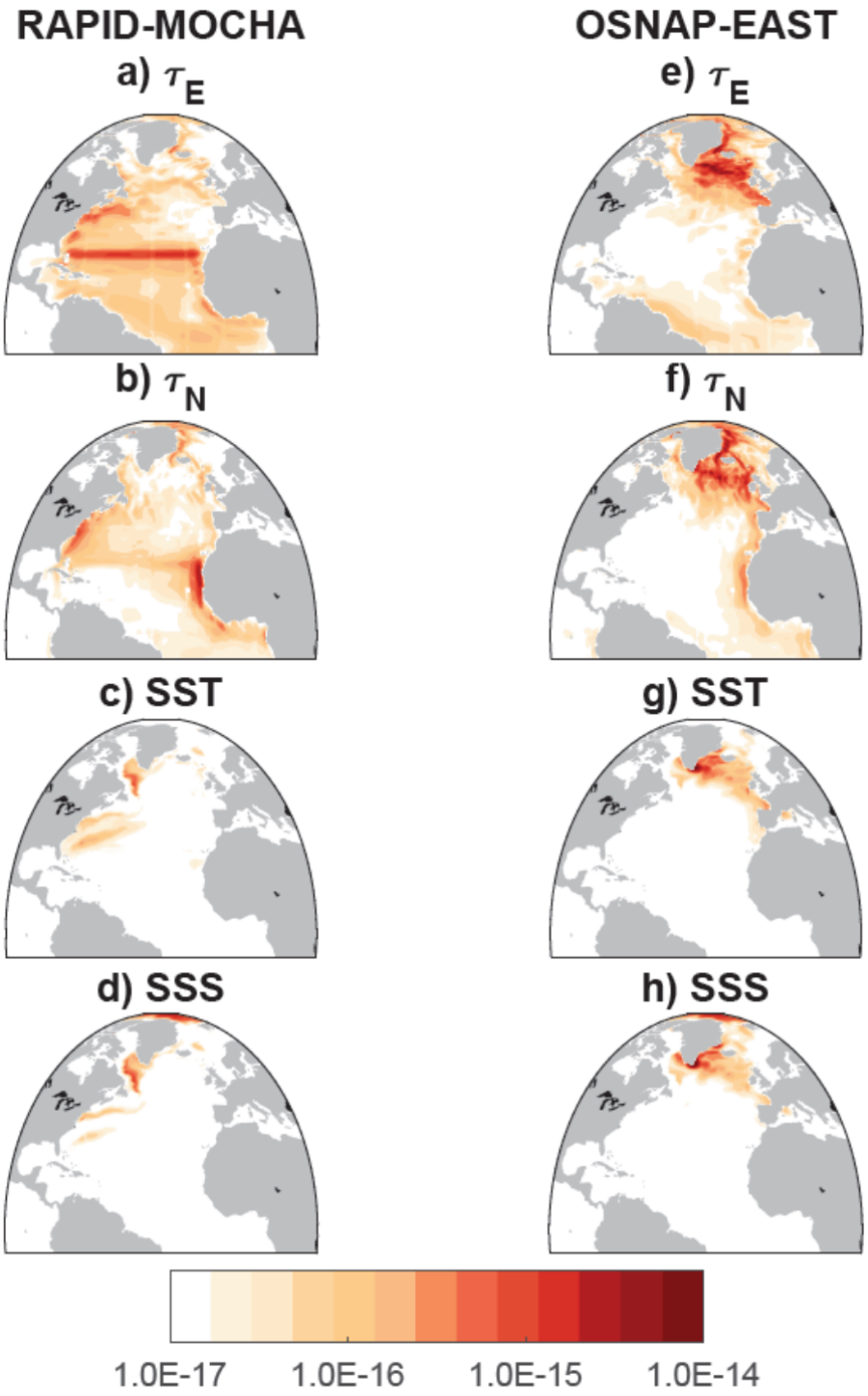

227

228 Figure 4. **Spatial origins of variability in overturning at the RAPID-MOCHA (a-d)**
229 **and OSNAP-EAST (e-h) arrays.** Color indicates the root-mean-square contribution
230 per unit area [Sv m^{-2}] to the convolutions in equation (1) over the period 1992-2015
231 using sensitivity patterns based on a linearization of the model over a historical period

232 (See Methods). Contributions due to zonal (a,e) and meridional (b,f) windstress, SST
233 (c,g), and SSS (d,h) all relative to the seasonal cycle. The scale is logarithmic.

234 Local winds dominate AMOC variability at 26°N (11) via two mechanisms: 1) Winds
235 generate meridional transport anomalies within the Ekman surface boundary layer (22); and
236 2) wind stress induces Rossby wave undulations of the thermocline that propagate westward
237 and cause density anomalies along the western boundary of the Atlantic (24). This build-up
238 of density anomalies alters the balance between east-west pressure gradients in the ocean and
239 the Coriolis force, thus changing the meridional transport (22) across the RAPID-MOCHA
240 array. Remote winds play a larger role in generating variability in the overturning across
241 OSNAP-EAST. For example, wind-driven coastal waves propagating along the boundaries
242 transmit the impact of variability in subtropical and subarctic wind stress to the Subpolar
243 North Atlantic (Figure 4f). These waves give rise to density anomalies on the Scottish and
244 Greenland shelves and hence affect the balance between ocean pressure gradients along the
245 OSNAP-EAST array and the Coriolis force. As a result, transport across the array changes. A
246 similar waveguide mechanism along the Atlantic's eastern boundary has also been identified
247 in studies exploring the sensitivity of Labrador Sea heat content (26), heat transport across
248 the Iceland-Scotland Ridge (27), and bottom pressure in the Arctic (28) to surface boundary
249 conditions.

250 The overturning at OSNAP-EAST is also strongly influenced by local SSS and SST
251 anomalies along the eastern coast of Greenland (Figure 4 g,h). This reflects two factors: (a)
252 the existence of large thermohaline variability in the region, and (b) the impact of density
253 anomalies at the boundary on the balance between ocean pressure gradients and the Coriolis
254 force. Note, however, that SST and SSS anomalies at these locations may be set by air-sea

fluxes of heat and freshwater over a much larger geographical area and over a period of several years (See Extended Data Figure ED4).

The buoyancy-forced component of the AMOC at 26°N exhibits long-term variability that arises from non-local surface buoyancy anomalies, namely those in the Arctic and the Labrador Sea (Figure 4c,d). Previous studies have suggested that deep convection in the Labrador Sea is related to subtropical AMOC variability on interannual and longer time scales (29, 30). We note that in the ECCO state estimate, there is deep convection both near the western boundary and in the interior of the Labrador Sea. However, the largest contribution of subpolar SST and SSS anomalies to reconstructed variability in RAPID-MOCHA overturning is concentrated in a narrow region near the western boundary of the subpolar basin (Figure 4c,d and Extended Data Figure ED5). This region is known to play a key role in the ventilation of deep water masses in the Labrador Sea (31). In contrast, surface buoyancy anomalies in the convective interior of the Labrador Sea make a smaller contribution to variability at RAPID-MOCHA. This result demonstrates that the causal connection between water mass transformation in the Labrador Sea and the subtropical AMOC is complex. As previously suggested (19), the background ocean circulation can advect density anomalies from the Labrador Sea towards the eastern subpolar gyre where they imprint (32) on Lower North Atlantic Deep Water (LNADW), the densest water mass in the AMOC lower limb. Anomalies in the volume and density of the LNADW layer can then be communicated to the subtropics at depth along the North Atlantic western boundary, and via ocean interior pathways, reaching 26°N on a timescale of approximately 4 years (33).

Implications for understanding future AMOC changes

Our analysis has shown that a large fraction of the observed and simulated variability in the Atlantic overturning circulation across the OSNAP-EAST array in the subpolar gyre,

279 and across the RAPID-MOCHA array at 26°N, can be reconstructed using best estimates of
280 historical SST, SSS, and wind anomalies, convolved with AMOC sensitivity patterns
281 computed from the adjoint of an ocean circulation model. This allows us to unambiguously
282 attribute recent historical changes to particular sources of variability. At 26°N, the impact of
283 remote (subpolar) surface buoyancy anomalies emerges only on decadal timescales (Figure
284 3b). On shorter timescales, almost all of the variability in overturning can be reconstructed
285 from knowledge of the past wind forcing alone (11, and see Figure 2d). However, our
286 analysis suggests that reconstructing and predicting the overturning at the latitude of the
287 OSNAP-EAST array presents a greater challenge because wind stress and surface buoyancy
288 anomalies each explain a comparable fraction of the total variability in the subpolar
289 circulation on inter-annual to decadal timescales. This provides strong motivation for
290 continued observation of the AMOC by the OSNAP array in order to monitor and understand
291 the state of the overturning circulation in that region and ultimately detect any anthropogenic
292 influence.

293 Our results also confirm that sustained observation of SST and SSS anomalies in the
294 subpolar North Atlantic, e.g. along the OSNAP-WEST line (see Figure 1 and Figure 4 c, d),
295 may give us predictability for the buoyancy-induced decadal trend in the subtropical AMOC
296 at the RAPID-MOCHA array. However, our reconstruction suggests that, compared to the
297 subtropics, the overturning circulation in the subpolar North Atlantic is more sensitive to
298 changes in the background ocean state (Figure 2, compare the size of the shaded gray
299 envelope of uncertainty in a and b) such as shifts in the sites of deep convection. This implies
300 that future climate change may alter the inter-annual variability in the OSNAP-EAST
301 overturning as well as its response to local and remote surface buoyancy anomalies.
302 Attributing, understanding, and predicting changes in AMOC transport at both subpolar and

subtropical latitudes therefore hinges on the continued observation of the overturning (3,4,5) and of the background ocean state (34) as part of a coordinated Atlantic observation system.

References

1. Lozier, M.S., 2012. Overturning in the North Atlantic. *Annual Review of Marine Science*, **4**, 291-315.
2. Stolpe, M., Medhaug, J. Sedláček , and R. Knutti (2018). Multidecadal Variability in Global Surface Temperatures Related to the Atlantic Meridional Overturning Circulation. *Journal of Climate*. **31**. 10.1175/JCLI-D-17-0444.1.
3. S.A. Cunningham, T. Kanzow, D. Rayner, M.O. Baringer, W.E. Johns, J. Marotzke, H. R. Longworth, E. M. Grant, J. J.-M. Hirschi, L. M. Beal, C. S. Meinen, H. L. Bryden, Temporal variability of the Atlantic meridional overturning circulation at 26.5°N. *Science* **317**, 935 – 938 (2007).doi:10.1126/science.1141304pmid:17702940
4. Smeed, D. A., Josey, S. A., Beaulieu, C., Johns, W. E., Moat, B. I., Frajka-Williams, E., et al. (2018). The North Atlantic Ocean is in a state of reduced overturning. *Geophysical Research Letters*, **45**, 1527– 1533. https://doi.org/10.1002/2017GL076350
5. M. Susan Lozier, S. Bacon, A. S. Bower, S. A. Cunningham, M. Femke de Jong, L. de Steur, B. deYoung, J. Fischer, S. F. Gary, B. J. W. Greenan, P. Heimbach, N.P. Holliday, L. Houpert, M.E. Inall, W.E.Johns, H.L. Johnson, J. Karstensen, F. Li, X. Lin, N. Mackay, D.P. Marshall, H. Mercier, P.G.Myeres, R.S. Pickart, H.R. Pillar, F. Straneo, V. Thierry, R.A. Weller, R.G. Williams, C. Wilson, J. Yang, J. Zhao, J. D. Zika,Overturning in the Subpolar North Atlantic Program: A new international ocean observing system. *Bull. Am. Meteorol. Soc*. **98**, 737 – 752 (2017). doi:10.1175/BAMS-D-16-0057.1

6. Biastoch, A., C. W. Böning, J. Getzlaff, J.-M. Molines, and G. Madec, 2008: Causes of interannual–decadal variability in the meridional overturning circulation of the North Atlantic Ocean. J. Climate, 21, 6599–6615, doi:10.1175/2008JCLI2404.1.
7. Polo, I., J. Robson, R. Sutton, and M. A. Balmaseda, 2014: The importance of wind and buoyancy forcing for the boundary density variations and the geostrophic component of the AMOC at 26°N. *J. Phys. Oceanogr.*, **44**, 2387–2408, https://doi.org/10.1175/JPO-D-13-0264.1
8. Ortega, P., Robson, J., Sutton, R.T. et al. (2017) Mechanisms of decadal variability in the Labrador Sea and the wider North Atlantic in a high-resolution climate model. . *Clim Dyn.,* **49**: 2625. https://doi.org/10.1007/s00382-016-3467-y
9. R.M. Errico. (1997) What is an adjoint model?, *Bull. Am. Meteorol. Soc*., **78**, 2577-2591, 10.1175/1520-0477(1997) 078<2577:WIAAM>2.0.CO;2
10. Forget, G., J.M. Campin, P. Heimbach, C.N. Hill, R.M. Ponte, and C. Wunsch, 2015: ECCO version 4: an integrated framework for non-linear inverse modeling and global ocean state estimation. *Geosci. Model Dev*., **8**, 3071-3104.
11. Pillar, H., P. Heimbach, H. Johnson, and D. Marshall, 2016: Dynamical attribution of recent variability in Atlantic overturning. *J. Climate*, 29, 3339-3352, doi:https://doi.org/10.1175/JCLI-D-15-0727.1.
12. Smith, T. and P. Heimbach. 2019. Atmospheric origins of variability in the South Atlantic meridional overturning circulation. *J. Clim*., **32(5),** 1483-1500, doi:10.1175/JCLI-D-18-0311.1.
13. Giering, R., 2010: Transformation of algorithms in Fortran Version 1.15 (TAF Version 1.9.70). FastOpt.

14. Fukumori, I., O. Wang, I. Fenty, G. Forget, P. Heimbach, and R. M. Ponte, 2017: ECCO Version 4 Release 3, http://hdl.handle.net/1721.1/110380, doi:1721.1/110380.

15. Marshall, J., C. Hill, L. Perelman, and A. Adcroft, Hydrostatic, quasi-hydrostatic, and nonhydrostatic ocean modeling, *J. Geophys. Res*., **102(C3)**, 5733-5752, 1997b

16. Forget, G., Ferreira, D., and Liang, X.: On the observability of turbulent transport rates by Argo: supporting evidence from an inversion experiment*, Ocean Sci.,* **11**, 839–853, https://doi.org/10.5194/os-11-839-2015, 2015

17. Fukumori, I., Heimbach, P., Ponte, R. M., and Wunsch, C. (2018). A dynamically consistent, multivariable ocean climatology. *Bull. Am. Meteorol. Soc*. **99**, 2107–2128. doi: 10.1175/BAMS-D-17-0213.1

18. Jackson, L. C., Dubois, C., Forget, G., Haines, K., Harrison, M., Iovino, D., et al. (2019). The mean state and variability of the North Atlantic circulation: A perspective from ocean reanalyses. *Journal of Geophysical Research: Oceans*, **124**, 9141–9170. https://doi.org/10.1029/2019JC015210

19. Lozier, M.S., Li, F., Bacon, S., Bahr, F., Bower, A. S., Cunningham, S. A., et al. (2019). A sea change in our view of overturning in the subpolar North Atlantic. *Science* **363**, 516–521. doi: 10.1126/science.aau6592

20. Li, F., M.S. Lozier and W. Johns, 2017. Calculating the meridional volume, heat and freshwater transports from an observing system in the subpolar North Atlantic: Observing system simulation experiment. *Journal of Atmospheric and Oceanic Technology*, doi: 10.1175/JTECH-D-16-0247.1

21. Desbruyères Damien, Mercier Herle, Maze Guillaume, Daniault Nathalie (2019). Surface predictor of overturning circulation and heat content change in the subpolar North Atlantic . Ocean Science , **15(3)**, 809-817. https://doi.org/10.5194/os-15-809-2019

373 22. Marshall, J., and A. Plumb (2008), *Atmosphere, Ocean, and Climate Dynamics: An*
374 *Introductory Text*, Elsevier, Amsterdam.
375 23. Menary, M. B., Hermanson, L., & Dunstone, N. J. (2016). The impact of Labrador Sea
376 temperature and salinity variability on density and the subpolar AMOC in a decadal
377 prediction system. Geophysical Research Letters, 43, 12,217–12,227.
378 https://doi.org/10.1002/2016GL070906
379 24. Zhao, J., & Johns, W. (2014b). Wind-forced interannual variability of the Atlantic
380 meridional overturning circulation at 26.5°N. *Journal of Geophysical Research:*
381 *Oceans*, **119(4)**, 2403–2419. https://doi.org/10.1002/2013JC009407
382 25. Kanzow, T. et al., 2010: Seasonal Variability of the Atlantic Meridional Overturning
383 Circulation at 26.5°N. *J. Climate*, **23**, 5678–5698,
384 https://doi.org/10.1175/2010JCLI3389.1.
385 26. Jones, D. C., Forget, G., Sinha, B., Josey, S. A., Boland, E. J. D., Meijers, A. J. S., et al.
386 (2018). Local and remote influences on the heat content of the Labrador sea: an adjoint
387 sensitivity study. *J. Geophys. Res. Oceans* **123**, 2646–2667. doi: 10.1002/2018JC013774
388 27. Loose, N., Heimbach, P., Pillar, H. R., & Nisancioglu, K. H. (2020). Quantifying
389 dynamical proxy potential through shared adjustment physics in the North
390 Atlantic. Journal of Geophysical Research: Oceans, 125,
391 e2020JC016112. https://doi.org/10.1029/2020JC016112
392 28. Fukumori, I., Wang, O., Llovel, W., Fenty, I., and Forget, G. (2015). A near-uniform
393 fluctuation of ocean bottom pressure and sea level across the deep ocean basins of the
394 Arctic Ocean and the Nordic Seas. *Progr. Oceanogr*. **134**, 152–172. doi:
395 10.1016/j.pocean.2015.01.013

29. Eden, C., J. Willebrand, Mechanism of interannual to decadal variability of the North Atlantic circulation. J. Clim. 14, 2266–2280 (2001). doi:10.1175/1520-0442(2001)014<2266:MOITDV>2.0.CO;2

30. Getzlaff, J., C. W. Böning, C. Eden, A. Biastoch, Signal propagation related to the North Atlantic overturning. Geophys. Res. Lett. 32, L09602 (2005). doi:10.1029/2004GL021002

31. MacGilchrist, G. A., H. L. Johnson, D. P. Marshall, C. Lique, M. Thomas, L. C. Jackson, and R. A. Wood, Locations and mechanisms of ocean ventilation in the high-latitude North Atlantic in an eddy-permitting ocean model. *J. Climate*, doi: https://doi.org/10.1175/JCLI-D-20-0191.1.

32. Zantopp, R., Fischer, J., Visbeck, M., and Karstensen, J. (2017), From interannual to decadal: 17 years of boundary current transports at the exit of the Labrador Sea, *J. Geophys. Res. Oceans*, **122**, 1724– 1748, doi:10.1002/2016JC012271.

33. Zou S, Lozier M.S., Buckley M. (2019) How is meridional coherence maintained in the lower limb of the Atlantic Meridional Overturning Circulation? *Geophys Res Lett* **46**:244–252. https://doi.org/10.1029/2018GL080958

34. Roemmich D., et al. (2019) On the Future of Argo: A Global, Full-Depth, Multi-Disciplinary Array. *Frontiers in Marine Science*, **6**, p. 439, DOI:10.3389/fmars.2019.00439

35. G.D. McCarthy, et al. (2015) Measuring the Atlantic Meridional Overturning Circulation at 26°N, *Progress in Oceanography*, **130**, 91-111, https://doi.org/10.1016/j.pocean.2014.10.006.

Acknowledgements

This study used the ARCHER UK National Supercomputing Service (http://www.archer.ac.uk). In our analysis, we apply the TAF software provided by FastOpt. The maps used in the figures and supplementary material were produced using the freely availabe software "M_Map: A mapping package for MATLAB", provided by R. Pawlowicz. We thank the groups that maintain the OSNAP and RAPID-MOCHA observational networks and the developers of the ECCO version 4 state estimate. Y.K. was funded by the OSNAP project through NERC grant, NE/K010948/1 and the TICTOC project through NERC grant NE/P019064/1. H.L.J., and D.P.M. were also funded by NERC grant, NE/K010948/1. G.F. acknowledges support from NASA award #6937342 and the Simons Foundation award #549931. P.H., H.R.P., and T.S. were supported in part by NOAA grant NOAA/NA130AR4310135, NSF grant NSF-OCE-1924546, and a JPL/Caltech subcontract. T.S. received additional funding from an Oden Institute CSEM fellowship. N.P.H. was funded by the OSNAP NERC grant NE/K010875/1. M.S.L and F.L. were supported by NSF grants OCE-1948335 and OCE-1924456. The authors thank the editor and the anonymous reviewers.

Ethics declarations

Competing interests

The authors declare no competing interests.

Code availability.

The code for the MITgcm and the scripts for post-processing model output are available at https://github.com/MITgcm/. The ECCO state estimate model configuration can be downloaded from https://github.com/gaelforget/ECCOv4, with initial and boundary conditions available at https://web.corral.tacc.utexas.edu/OceanProjects/ECCO/ECCOv4. The TAF algorithmic differentiation software is proprietary and provided by FastOpt. Code used to process data and produce figures is available from the corresponding author Y.K. upon reasonable request.

Data availability

The OSNAP data products are publicly available at www.o-snap.org. The derived data including the OSNAP-EAST overturning are furthermore available in Duke Digital Repository, https://research.repository.duke.edu/collections/1z40kt318. The RAPID-MOCHA overturning timeseries is available at https://www.rapid.ac.uk/rapidmoc/rapid_data/datadl.php

Contributions

All authors discussed the results and contributed to the preparation of the final manuscript. Y.K. took the lead in writing the text while holding regular discussions with H.L.J., D.P.M., T.S., and H.P. Y.K. planned, designed, and performed the adjoint sensitivity analysis with the MITgcm. P.H. and G.F. developed and maintained the ECCO version 4 state estimate and the associated tools for post-processing MITgcm output on an irregular grid. T.S. adapted the MITgcm diagnostic package. N.P.H., F.L., and M.S.L. developed and applied the data analysis methodology for OSNAP observations, and F.L. provided the OSNAP-EAST overturning time series.

METHODS

We use an algorithmic differentiation software, Transformation of Algorithms in FORTRAN (TAF, 1), to obtain the adjoint of the MIT ocean general circulation model (MITgcm) in the ECCO (Estimating the Circulation and Climate of the Ocean) version 4 (v4) configuration (2), whose release 3 covers the 1992-2015 period. The ECCOv4 state estimate reproduces very skillfully the observed subtropical AMOC at the RAPID-MOCHA array (Rapid Climate Change Array – Meridional Overturning Circulation and Heatflux Array). If we detrend and smooth the intermonthly timeseries with a twelve-month running mean, the correlation between the state estimate and the RAPID-MOCHA observations is R=0.83 (significant at the 1% level). In terms of the low-frequency variability, the RAPID-MOCHA overturning represented in ECCOv4 does not show the same 2004-2006 positive anomaly as in the direct observational estimate. Hence, ECCOv4 underestimates the subsequent decline at RAPID-MOCHA after 2006. Furthermore, towards the end of the observational record, there is a mismatch in the high frequency variability between ECCOv4 and RAPID-MOCHA observations despite the good agreement overall. The OSNAP (Overturning in the Subpolar North Atlantic Program) observational record is too short to compute correlations with the ECCO historical state estimate. However, the ECCO timeseries mostly agree with the direct observational estimate at OSNAP-EAST within the observational uncertainty.

In this study, we modify the adjoint code of the MITgcm ECCO configuration and set up numerical calculations that output sensitivity patterns for the response of the Atlantic overturning to SST and SSS, as well as the response to surface wind stress assuming constant SST and SSS, at different lead times. Our objective functions for each adjoint calculation are defined in terms of volume transport in Sverdrups (1 Sv = 10^6 m^3s^{-1}).

We compute seasonal sensitivity patterns of the February, May, August, and November monthly-averaged overturning and for computational efficiency assume these to be representative of the winter, spring, summer, and fall objective functions, respectively. This simplification introduces an annually cyclic bias in the buoyancy-related components of our reconstruction (see the apparent small oscillation in Figure 3 of the main text). Nevertheless, it is clear to see that the oscillations that arise due to this computational choice are small and with nearly compensating effects in the SST and SSS components. Hence, this does not affect our conclusions.

We perform two sets of adjoint calculations each yielding the seasonally-dependent linear sensitivity of the overturning at two different regions in the North Atlantic. First, we perform a set of calculations that give us the lagged sensitivity of the AMOC volume transport at 26°N in depth space to surface anomalies at different lead times and horizontal locations. Calculations for the AMOC strength at 26°N in potential density space give similar sensitivity results. Second, we perform an analogous set of calculations for the lagged sensitivity of the density-space overturning across the OSNAP-EAST line. To be consistent with observational products from the OSNAP array, we use potential density coordinates, referenced to the surface. The Eulerian velocity components at the vertical walls of each model grid cell are binned into different layers depending on the potential density interpolated onto the cell boundaries. We then obtain the OSNAP-EAST overturning by integrating the velocity across the array vertically, going from denser to lighter layers.

The sensitivity patterns we obtain depend on the time-evolving ocean state about which we linearize the model. To assess this non-linear effect, we compute each set of sensitivity patterns twice, linearizing about two different periods of the ECCO state estimate: one ending in 2001-2002 and one in 2006-2007. We select these two representative periods, ending 10 and 15 years into the ECCO run, because the earlier years of the state estimate are marked by unusually strong convection in the subpolar North Atlantic. Computational cost limits our ability to repeat the

adjoint calculation over additional time periods. We consider both the mean and the spread between the two estimates and use each of them to reconstruct the AMOC timeseries and to identify sources of variability in Atlantic overturning. Figures 3 and 4 in the Main Text show sources of variability in the AMOC based on a linearization of the model over the historical period ending in 2006-2007. In comparison, Figure S2 in the SI presents an analogous estimate but using a linearization over the earlier time period ending in 2001-2002. When computing correlations, we use the mean of the two reconstructions.

In our reconstructions we consider sensitivity to SST and SSS, rather than fluxes of heat and freshwater across the air-sea interface, because the former are more readily constrained by available in-situ and satellite observations of the ocean. Moreover, air-sea fluxes are a step further removed from surface buoyancy compared to temperature and salinity. The ocean integrates local and remote surface fluxes, which then gives rise to SST and SSS anomalies. Therefore, if we used AMOC sensitivity to surface fluxes, we would have to consider much longer lead times, at which the adjoint of the MITgcm becomes less reliable (see a discussion in 3). For example, we would need accurate sensitivity to surface fluxes all along the Gulf Stream and the North Atlantic Current advective pathways going back years (See Extended Data Figure ED4).

We convolve the sensitivity patterns from each set of adjoint calculations with 1992 – 2015 historical estimates of wind stress, SST, and SSS anomalies from the ECCO ocean state estimate. We define anomalies in these fields relative to the climatological seasonal cycle. However, when exploring the wind contribution to AMOC variability, we also separately consider the impact of the climatological seasonal cycle in surface wind stress. Each convolution gives us an estimate for the time-evolving contribution $C_{\mathcal{P}}$ of a given ocean surface field $\mathcal{P}$ to historical variability in the rate of overturning:

$$C_{\mathcal{P}}(t) = \int_{t-\tau}^{t} \int \mathcal{P}(\boldsymbol{x}, t')\, \mathcal{G}_{\mathcal{P}}(t; \boldsymbol{x}, t - t')\, d\boldsymbol{x}\, dt' \qquad \text{(S1)}$$

where $\mathcal{P}$ is the surface field anomaly relative to the climatological monthly mean. The function $\mathcal{G}_{\mathcal{P}}$ denotes the sensitivity pattern that depends on the season at time t, the lead time t', and the geographical location $\boldsymbol{x}$. In order to remove numerical noise, the patterns of sensitivity to SST and SSS are smoothed using a diffusive Gaussian operator (3,4) with a spatial decorrelation scale of two grid cells. This operator is not applied to wind stress sensitivity patterns, vector fields on an irregular model grid. The integration in space $\boldsymbol{x}$ is over the whole global ocean surface, and the time integration goes back to a cutoff lead time τ representing the assumed maximum memory of the AMOC to past forcing. The cutoff lead times are as follows: 3 years for wind stress in OSNAP-EAST reconstructions, 2 years for SST and SSS in OSNAP-EAST reconstructions, and 6 years for all components in RAPID AMOC reconstructions. In reality, the ocean circulation retains memory of previous forcing on much longer timescales. However, nonlinear effects are larger at longer lead times and the adjoint of the MITgcm cannot capture them (see a discussion in 5). By sweeping parameter space in t', we have established that when we increase the cutoff lead times beyond the appropriate ranges we identify, our reconstruction skill decreases. This is likely due to the growth of nonlinear error terms at longer lead times. On the other hand, cutoff lead times that are unnecessarily short lead to omission of useful information about past forcing.

When computing the contributions due to wind stress, we use AMOC sensitivity patterns representative of 5-day steps in lead-time. We convolve these sensitivity patterns with 5-day mean wind stress fields from ECCO. When estimating the contributions due to surface buoyancy, we use 10-day means for the SST, the SSS, and the corresponding sensitivity patterns averaged over 10-day lead-time windows. Even though the ECCO configuration is nominally at a 1°×1° horizontal resolution, we need this sub-monthly temporal resolution because of the high-frequency, spatially localized wintertime convective variability in the subpolar North Atlantic. Summing the contributions due to wind stress, SST, and SSS anomalies provides a partial reconstruction of the

historical variability in the Atlantic overturning circulation relative to the seasonal cycle. Finally, we combine our reconstruction with the 1992-2015 climatological seasonal cycle in Atlantic overturning based on the ECCO state estimate. Note that the OSNAP-EAST observational record is too short to estimate the background seasonal climatology in overturning. Furthermore, analysis of the OSNAP-EAST timeseries in ECCO suggests that variability relative to the seasonal cycle is comparable in amplitude to the seasonal cycle in subpolar overturning.

In this study, we identify the regions where variability in wind stress, SST, and SSS most strongly projects on the corresponding AMOC sensitivity patterns and activates them. We consider the root-mean-square contribution per unit area [Sv m^{-2}] to the convolutions in equation (1) over the period 1992-2015:

$$C_{\mathcal{P}}(\boldsymbol{x}) = \frac{1}{A(\boldsymbol{x})}\sqrt{\frac{1}{(T_f \cdot \tau)}\sum_{t=0}^{T_f}\sum_{t'=\max(t-\tau,0)}^{t}\left[\mathcal{P}(\boldsymbol{x},t')\,\mathcal{G}_{\mathcal{P}}(t;\boldsymbol{x},t-t')\right]^2} \qquad \text{(S2)}$$

where $A(\boldsymbol{x})$ is the horizontal surface area of the model grid cell in location $\boldsymbol{x}$, $\mathcal{P}$ represents the surface field anomalies relative to the climatology at a lead time t' summed up to a finite maximum memory τ, as in equation (S1). The function $\mathcal{G}_{\mathcal{P}}$ is the corresponding sensitivity pattern that depends on the season, as in equation S1 in the Methods. We sum the convolution of $\mathcal{P}$ and $\mathcal{G}_{\mathcal{P}}$ until the end of the available timeseries $t = T_f$ and compute the root-mean-square.

We acknowledge that the AMOC sensitivity patterns, reconstructions, and attributions presented here are based on a model that approximates processes in the ocean. For example, the regions of deep wintertime convection in the North Atlantic are known to differ widely across climate models (6). Moreover, the ECCO configuration of the MITgcm that we use does not resolve mesoscale ocean eddies whose important role in the circulation is instead represented via a widely used parameterization. Nevertheless, since ECCO formally calibrates the spatially varying

584 parameters in the model's eddy transport scheme using observational constraints (7), the evolving
585 state of the ocean in ECCO closely tracks historical temperature, salinity, and ocean circulation
586 conditions (8).

587 We compare our model-based results with observational data from the RAPID-MOCHA
588 array at 26°N and the OSNAP arrays in the subpolar North Atlantic.

589 In the subpolar latitudes, recent and pre-existing OSNAP moorings on the basin boundaries
590 measure temperature, salinity, density, and velocity (9,10). Away from the OSNAP moorings, an
591 objective analysis method is used to interpolate between these measurements using data from Argo
592 profiles (e.g., 11) and OSNAP gliders, as well as World Ocean Atlas 2013 climatology (12). In
593 addition, away from the arrays, Ekman velocities are estimated from ERA-Interim wind fields (13).
594 This wind-driven ageostrophic transport is assumed to be confined to the Ekman surface boundary
595 layer (14). Geostrophic velocity (14) is estimated using two different reference velocities. Wherever
596 deep moorings are available, their velocity measurements are used as a reference, except in the
597 western Labrador Sea and the central Iceland Basin. Otherwise, time-mean surface velocity data
598 from satellite altimetry provides the reference velocity. Finally, to guarantee a zero net mass transport
599 across the entire OSNAP array, a compensation transport term is included at OSNAP-WEST at each
600 time step. The same term is added with the opposite sign across OSNAP-EAST. These
601 compensation terms are distributed uniformly in regions where velocity measurements are not
602 available.

603 We furthermore use publicly available observational data for the subtropical AMOC
604 provided by the RAPID project (15). We bin the RAPID-MOCHA overturning time series
605 into the same 30-day windows as our model output and reconstructions.

606 When comparing timeseries from the state estimate, reconstructions, and observations, we
607 compute correlation coefficients using standard methods for linear regression. When we test the

significance of the regression coefficients, we take into account the redness in the spectral properties of the timeseries. Thus, our null hypothesis is not based on a standard normal distribution. Instead, we use an established spectral Monte-Carlo approach for significance testing (16, 17). All regression coefficients cited in this study are significant at the 1% level.

References for the Methods Section

1. Giering, R., 2010: Transformation of algorithms in Fortran Version 1.15 (TAF Version 1.9.70). FastOpt.
2. Fukumori, I., O. Wang, I. Fenty, G. Forget, P. Heimbach, and R. M. Ponte, 2017: ECCO Version 4 Release 3, http://hdl.handle.net/1721.1/110380, doi:1721.1/110380.
3. Kostov, Y., Johnson, H.L. & Marshall, D.P. AMOC sensitivity to surface buoyancy fluxes: the role of air-sea feedback mechanisms. Clim Dyn 53, 4521–4537 (2019). https://doi.org/10.1007/s00382-019-04802-4
4. Weaver AT, Courtier P (2001) Correlation modelling on the sphere using a generalized diffusion equation. QJR Meteorol Soc 127:1815–1846
5. Smith, T. and P. Heimbach. 2019. Atmospheric origins of variability in the South Atlantic meridional overturning circulation. *J. Clim*., **32(5)**, 1483-1500, doi:10.1175/JCLI-D-18-0311.1.
6. Heuzé, C. North Atlantic deep water formation and AMOC in CMIP5 models. *Ocean Sci.* **13**, 609–622 (2017).
7. Forget, G., J.M. Campin, P. Heimbach, C.N. Hill, R.M. Ponte, and C. Wunsch, 2015: ECCO version 4: an integrated framework for non-linear inverse modeling and global ocean state estimation. *Geosci. Model Dev*., **8**, 3071-3104.

8. Forget, G., Ferreira, D., and Liang, X.: On the observability of turbulent transport rates by Argo: supporting evidence from an inversion experiment*, Ocean Sci.,* **11**, 839–853, https://doi.org/10.5194/os-11-839-2015, 2015.
9. Lozier, M.S., Bacon, S., Bower, A. S., Cunningham, S. A., Femke de Jong, M., de Steur, L., et al. (2017). Overturning in the Subpolar North Atlantic Program: A new international ocean observing system*. Bulletin of the American Meteorological Society*, **98(4)**, 737–752. https://doi.org/10.1175/BAMS-D-16-0057.1
10. Zantopp, R., Fischer, J., Visbeck, M., and Karstensen, J. (2017), From interannual to decadal: 17 years of boundary current transports at the exit of the Labrador Sea, *J. Geophys. Res. Oceans*, **122**, 1724– 1748, doi:10.1002/2016JC012271.
11. Forget, G., H. Mercier, B. Ferron (2008) Combining Argo profiles with a general circulation model in the North Atlantic. Part 2: Realistic transports and improved hydrography, between spring 2002 and spring 2003. *Ocean Modelling*, **20**, Issue 1, 17-34, https://doi.org/10.1016/j.ocemod.2007.06.002.
12. Locarnini, R. A., A. V. Mishonov, J. I. Antonov, T. P. Boyer, H. E. Garcia, O. K. Baranova, M. M. Zweng, and D. R. Johnson (2010), *World Ocean Atlas 2009*, vol. 1, Temperature, Atlas NESDIS **68**, edited by S. Levitus, NOAA, U.S. Gov. Print. Off., Washington, D. C.
13. Dee, D. P., Uppala, S. M., Simmons, A. J., Berrisford, P., Poli, P., Kobayashi, S, et al. (2011). The ERA-Interim reanalysis: Configuration and performance of the data assimilation system. *Quarterly Journal of the Royal Meteorological Society*, **137**, 553–597. https://doi.org/10.1002/qj.828
14. Marshall, J., and A. Plumb (2008), *Atmosphere, Ocean, and Climate Dynamics: An Introductory Text*, Elsevier, Amsterdam.

15. Smeed, D. A., Josey, S. A., Beaulieu, C., Johns, W. E., Moat, B. I., Frajka-Williams, E., et al. (2018). The North Atlantic Ocean is in a state of reduced overturning. *Geophysical Research Letters*, **45**, 1527– 1533. https://doi.org/10.1002/2017GL076350
16. Lund, I. A., 1970: A Monte Carlo method for testing the statistical significance of a regression equation. J. Appl. Meteor., 9, 330–332, https://doi.org/10.1175/1520-0450(1970)009<0330:AMCMFT>2.0.CO;2.
17. Cornish, S. B., Y. Kostov, H. L. Johnson, and C. Lique, 2020: Response of Arctic Freshwater to the Arctic Oscillation in Coupled Climate Models. J. Climate, 33, 2533–2555, https://doi.org/10.1175/JCLI-D-19-0685.1.

EXTENDED DATA FIGURES

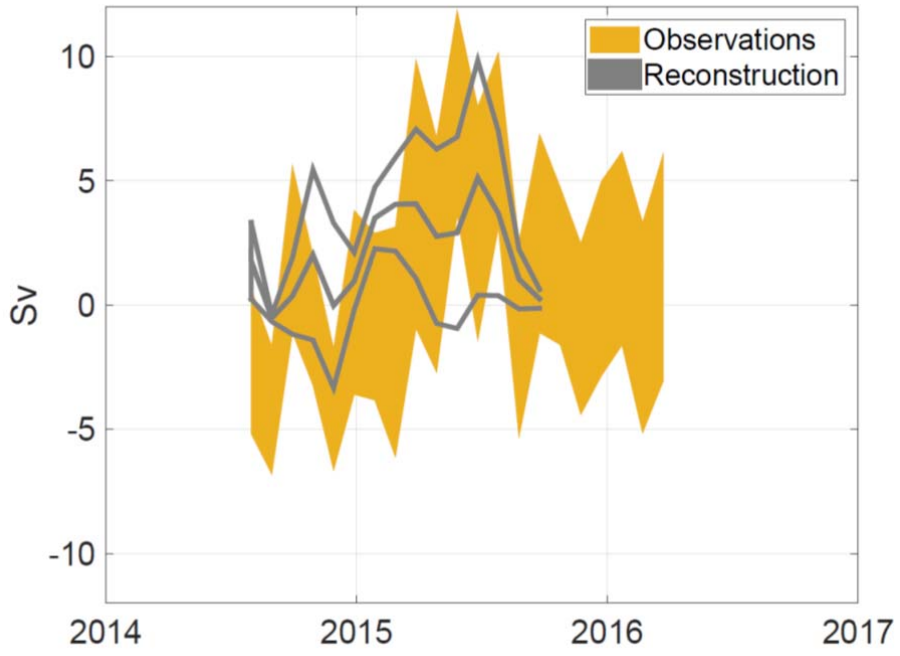

Figure ED1. Reconstruction skill for OSNAP-EAST observations. Comparison between observations (yellow envelope showing ±1 standard deviation of the observational uncertainty) and our two reconstructions (outer gray contours) of OSNAP-EAST overturning [Sv] based on two different sets of sensitivity patterns: one set from objective functions in 2001-2002, and a second set from objective functions in 2006-2007. The reconstructions are interpolated onto the same 30-day windows as the observations. We consider both the mean of our two reconstructions (middle gray contour) and the spread between them (outer gray contours). Note that

our reconstruction estimate uses the ECCOv4r3 mean seasonal cycle, since the observational record at OSNAP-EAST is short.

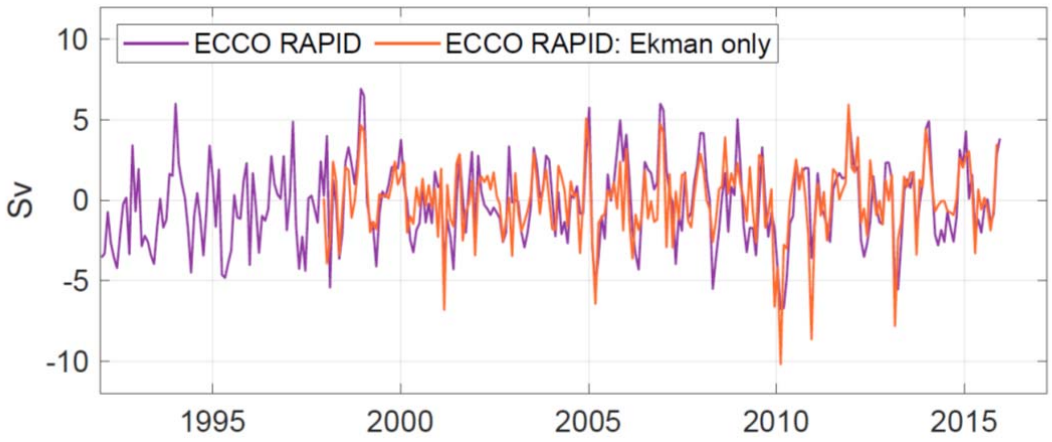

Figure ED2. Ekman transport contribution to overturning variability at RAPID-MOCHA in ECCO. ECCO-based comparison between variability in RAPID-MOCHA overturning (purple) and Ekman transport variability at 26°N (orange) over the time-period of the linear reconstructions in the main text. Anomalies are shown relative to the long-term mean.

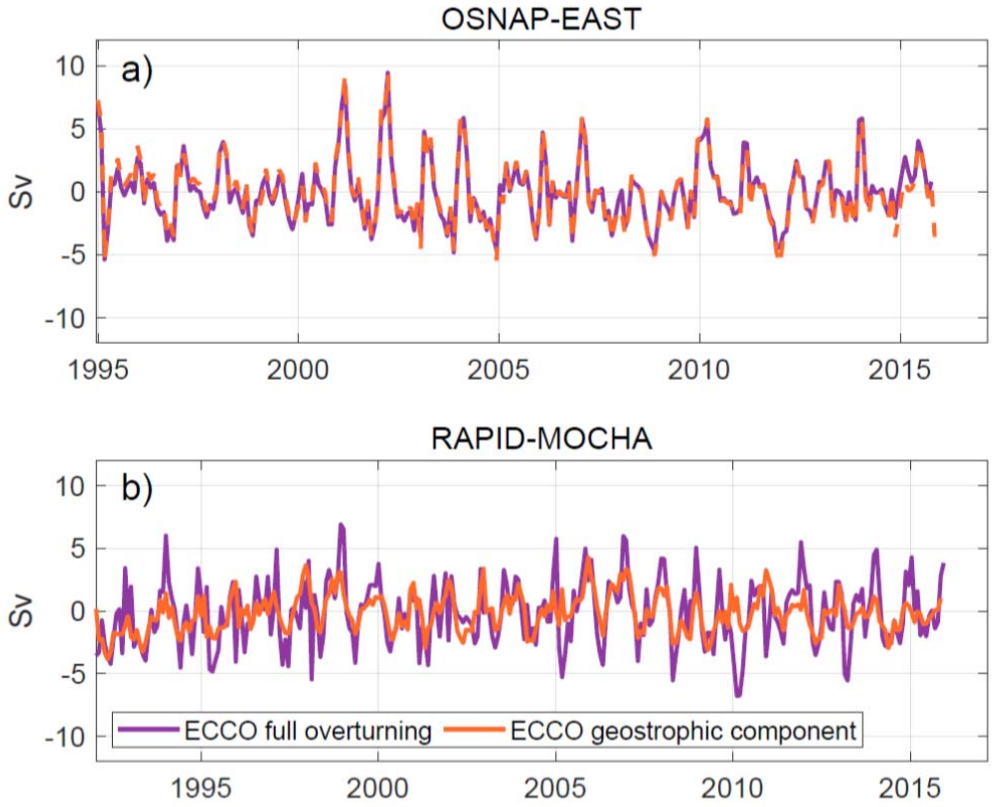

Figure ED3. Geostrophic component of overturning in the North Atlantic. Overturning variability (purple, volume transport in Sv) at OSNAP-EAST (a) and RAPID-MOCHA (b) in the ECCO state estimate contrasted against variability in the geostrophic component of overturning (orange). The comparison spans the time-period of the linear reconstructions in the main text. Anomalies are shown relative to the long-term mean.

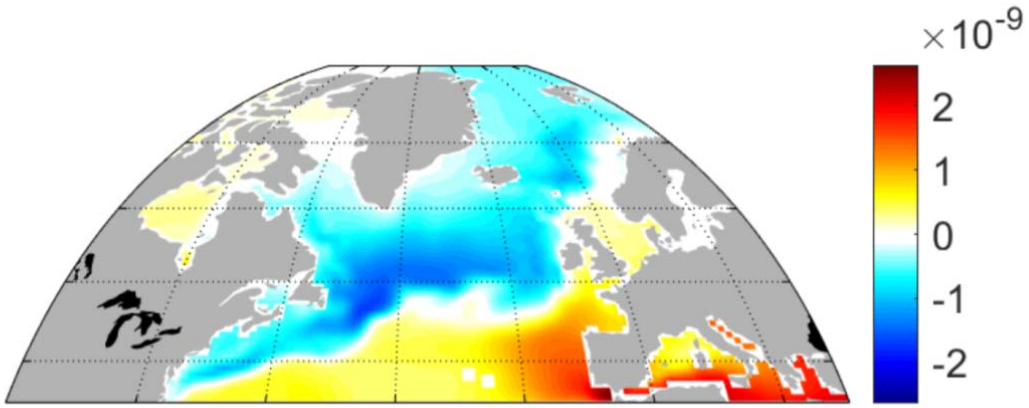

Figure ED4. Sensitivity of the OSNAP-EAST overturning to surface heat fluxes. Sensitivity of the OSNAP-EAST overturning in February 2007 to net surface heat fluxes [Sv per (W m^{-2} sustained over 1 hour)] at a lead time of **nine** years. Red shading indicates that heat flux into the ocean contributes to a delayed strengthening of the OSNAP-EAST overturning 9 years later. Blue shading indicates that cooling the ocean surface at that lead time causes a lagged strengthening of the OSNAP-EAST overturning. Notice the pattern tracking the Gulf Stream – North Atlantic Current advective pathway from the Caribbean to the subpolar latitudes. This *long memory* of past sea surface fluxes motivates the use of AMOC sensitivity to SST and SSS instead.

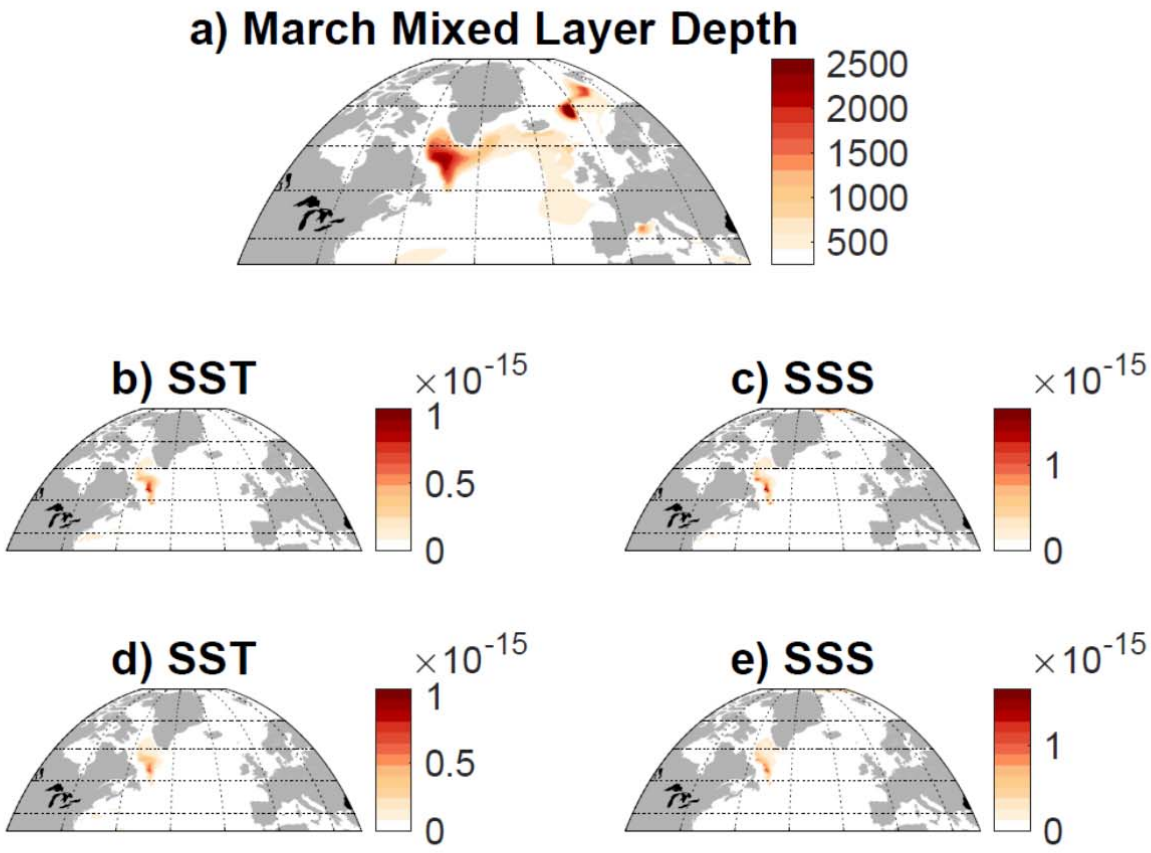

721

722 **Figure ED5. North Atlantic deep convection and spatial origins of buoyancy-**
723 **driven variability in RAPID-MOCHA overturning.** (a) Climatological March mixed
724 layer depth [m] in ECCO; (b-e) Spatial sources of variability in the RAPID-MOCHA
725 AMOC overturning: root-mean-square contribution per unit area [Sv m^{-2}] to the
726 convolutions in equation (1) of the main text over the period 1992-2015 using
727 sensitivity patterns based on (b,c) 2006-2007 and (d,e) 2001-2002 AMOC objective
728 functions. Contributions due to SST (b,d), and SSS (c,e) all relative to the seasonal
729 cycle. The scale in all panels is linear.